Title
Dynamic Simulation of an Integrated Solid Oxide Fuel Cell System Including Current-Based Fuel Flow Control

Journal
Journal of Electrochemical Energy Conversion and Storage, 3(2)

ISSN
1550-624X

Authors
Mueller, Fabian
Brouwer, Jacob
Jabbari, Faryar
et al.

Publication Date
2006-05-01

DOI
10.1115/1.2174063

Dynamic Simulation of an Integrated Solid Oxide Fuel Cell System Including Current-Based Fuel Flow Control

Fabian Mueller
e-mail: fm@nfcrc.uci.edu

Jacob Brouwer
e-mail: jb@nfcrc.uci.edu

Faryar Jabbari
e-mail: fjabbari@uci.edu

Scott Samuelsen
e-mail: gss@uci.edu

Mechanical and Aerospace Engineering Department,
National Fuel Cell Research Center,
University of California,
Irvine, CA 92697

A two-dimensional dynamic model was created for a Siemens Westinghouse type tubular solid oxide fuel cell (SOFC). This SOFC model was integrated with simulation modules for other system components (e.g., reformer, combustion chamber, and dissipater) to comprise a system model that can simulate an integrated 25 kw *SOFC system located at the University of California, Irvine. A comparison of steady-state model results to data suggests that the integrated model can well predict actual system power performance to within 3%, and temperature to within 5%. In addition, the model predictions well characterize observed voltage and temperature transients that are representative of tubular SOFC system performance. The characteristic voltage transient due to changes in SOFC hydrogen concentration has a time scale that is shown to be on the order of seconds while the characteristic temperature transient is on the order of hours. Voltage transients due to hydrogen concentration change are investigated in detail. Particularly, the results reinforce the importance of maintaining fuel utilization during transient operation. The model is shown to be a useful tool for investigating the impacts of component response characteristics on overall system dynamic performance. Current-based flow control (CBFC), a control strategy of changing the fuel flow rate in proportion to the fuel cell current is tested and shown to be highly effective. The results further demonstrate the impact of fuel flow delay that may result from slow dynamic responses of control valves, and that such flow delays impose major limitations on the system transient response capability.* [DOI: 10.1115/1.2174063]

Keywords: SOFC, integrated system, dynamic simulation, data comparison, fuel cell system control, dynamic response

Introduction and Background

Solid oxide fuel cells (SOFC) generate electricity in a fuel efficient and environmentally friendly fashion, and are being widely considered for power generating technology in a broad array of applications. Many emerging SOFC applications will require the ability of SOFC systems to follow very fast load transients. One such example includes large scale distributed generation where it has been identified that slow SOFC response time can lead to instability of the utility grid distribution system [1]. Stand-alone (without grid connection) power generation for buildings or other loads will require fast fuel cell system dynamic response capabilities, as well. Other applications requiring fast SOFC system transient capability include auxiliary power unit (APU) systems that power dedicated loads onboard vehicles for naval, land, and aerospace applications [2–4].

In order to improve SOFC system load following capability, one must have tools that can provide insight and understanding into the characteristics of transients of SOFC systems. This has led to a substantial computational and experimental effort to understand SOFC transients [5–10]. Most generally, SOFC stacks have been identified as having three characteristic response times governed by different mechanisms. One is governed by the electrochemistry and current converter electronics, with a characteristic response time on the order of milliseconds, another is due to hydrogen composition changes within the fuel cell on the order of seconds, and a third is the cell mass temperature change, with characteristic response times on the order of minutes to hours [10].

In the present work a MATLAB SIMULINK® dynamic model of a Siemens Westinghouse 25 kW fuel cell system, located at the National Fuel Cell Research Center, Irvine, California was developed. The model simulates the detailed electrochemical performance of a tubular SOFC stack integrated with a steam reformer, combustor, and dissipater. The system model is useful to garner physical understanding of system level transients and design control strategies to improve SOFC system transient load following capability. The work focuses on the dynamics of hydrogen flow in SOFC systems during transient load following. Fuel starvation within the cells is a major limiting factor in SOFC system load following capability, as the dynamics of the current converter are too fast to be significant and the dynamics for full stack or system temperature change have very large time scales that can be controlled by air flow rates.

Model Description

Integrated SOFC System. The primary components of the physical system are four annular reformers, a SOFC stack comprised of 576 SOFC tubular cells, a combustor, an air recuperator, a blower, and a current converter. The system modeled accounts for the integration of the reformer, stack, and combustor of the experiment as illustrated in Fig. 1. More detailed system schematics and information regarding the integrated SOFC system can be found in [11,12]. There are many interactions between the flows of each component in the system. Of course, the reformer provides a hydrogen-rich reformate gas to the fuel cell. Following the

Manuscript received July 19, 2005; final manuscript received October 11, 2005. Review conducted by Subhash C. Singhal.

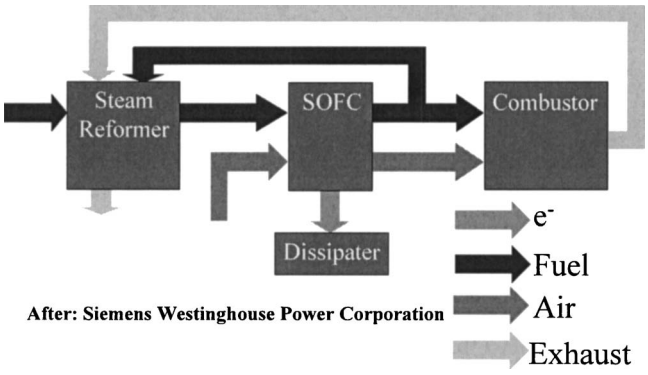

Fig. 1 Flow schematic of 25 kW integrated system model, after Siemens Westinghouse Power Corporation

fuel cell, a portion of the anode off gas is recirculated to the reformer, providing the required steam and some thermal energy for reformation. The remaining anode stream is mixed with the cathode depleted air stream, and is completely oxidized at temperatures above the autoignition temperature. The combustor exhaust is recirculated through the reformer to provide heat to counterbalance the endothermic steam reformation chemical reactions.

Modeling Methodology. The system dynamic model is developed in SIMULINK® using a methodology that develops a discretized physical model for the external steam reformer, fuel cell stack, and combustor components of the system. Each of the component models are then linked together to represent the entire system. In this fashion interactions among system components are captured to simulate the system dynamic response.

All geometric features or all physical and chemical processes occurring in the components could not be captured without becoming too computationally intensive. Thus, simplifying assumptions and simplifications had to be made to enable solution of the dynamic equations that govern fuel cells at the system level.

The simplifications employed in this case include a quasi-two-dimensional approach for resolving geometrical features of the major system components. This approach discretizes each of the major component models in the primary flow direction and resolves physical and chemical processes such as heat transfer, chemical reaction, and ion flow as they occur in the cross-wise direction. The discretized elements in the flow direction are called nodes. Each node is comprised of several control volumes representing the primary elements in the cross-wise direction.

Within each control volume only the physical and chemical processes that affect the time scale of interest in the dynamic simulation are considered ($>$10 ms). For example, processes such as electrochemical reaction rates and electric current flow dynamics are assumed to occur at a time scale that is faster than that of interest to the model. Several additional assumptions are made in the development of the set of equations that is solved for in each of the control volumes. This common set of assumptions is presented in the next section.

Assumptions

1. One-dimensional fully developed laminar flow along the stream-wise direction.
2. Control volumes are characterized by a single lumped temperature, pressure, and species mole fractions condition.
3. All gases are ideal gases.
4. No heat transfer to the environment. The system is assumed to be well insulated from the environment.
5. No carbon formation or deposition is considered in the chemical or electrochemical reaction models.
6. The gas in the system is assumed to be incompressible since the Mach number through out the system is small ($<$0.2). Also a constant pressure drop governs the momentum conservation throughout each simulation module.
7. The gas kinematic viscosity and thermal conductivity used to calculate heat transfer coefficients in the annular steam reformer are evaluated by assuming the combustor exhaust stream is air and the reformate stream is steam each evaluated at the local temperature.
8. The reformer catalyst bed and the adjoining containment vessels (steel cans) have a lumped temperature. (The respective Biot number was found to be 0.01, which is much less than the required 0.1 for this assumption.)
9. The reformer cans are assumed to be a thin stainless steel sheet that only serves to separate the gas/catalyst control volumes.
10. Each cell in the stack is assumed to operate identically, so that a single tubular SOFC simulation is taken as representative and used to calculate full stack performance [13,14].
11. All electrodes are good conductors for which an equipotential electrode surface is assumed [14].
12. Quasisteady electrochemistry is assumed, since the electrochemistry is rapid (on the order of 10^{-3} sec) in comparison to the system transients of interest [15].
13. Activation polarization in the anode is neglected. Activation polarization in the cathode is an order of magnitude higher than in the anode [16,17]. A single activation polarization equation is used to capture the effects of all physical and chemical processes that polarize the charge transfer process.
14. In the fuel cell, all reactants generate their ideal number of electrons, and no fuel or oxidant crosses the electrolyte.
15. Only hydrogen reaction with oxygen contributes to a voltage. It is assumed that oxygen ions preferably react with hydrogen over carbon monoxide.

General Equations. The general equations used throughout the model are described in this section. Each of the individual component models is constructed in a similar manner. The dynamic conservation equations, primary heat transfer equations, and equations of state that are solved in each of the control volumes are derived from the same general equations. The details of equations as they are applied to the control volumes of each component model are then described in the component model subsections.

Solid Control Volume Equations. Within each component it is important to resolve the temperature of each solid control volume to evaluate heat transfer, as well as the performance of the fuel cell. The temperature of each solid control volume in the system is determined by the following conservation of energy equation:

$$\rho VC\frac{dT}{dt} = \sum \dot{Q}_{\text{in}} - \sum \dot{W}_{\text{out}} \tag{1}$$

Equations of Heat Transfer Between Control Volumes. Fourier's law is utilized to capture conduction heat transfer between solid control volumes using the temperature of each control volume

$$\dot{Q}_{\text{cond}} = \frac{A \cdot k_s \cdot (T_2 - T_1)}{L} \tag{2}$$

and Newton's law is utilized to determine convection heat transfer between solid and gas control volumes

$$\dot{Q}_{\text{conv}} = A \cdot h \cdot (T_2 - T_1) \tag{3}$$

The heat transfer parameters and network vary for each component model and will be described in detail for each.

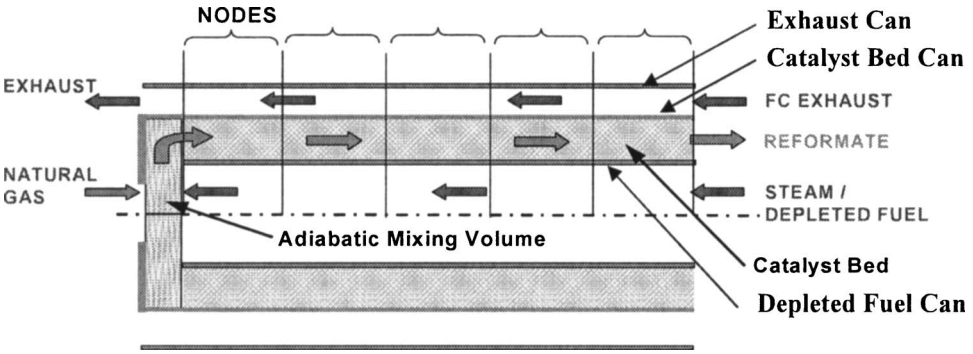

Fig. 2 Schematic of the annular geometry external steam reformer, showing model nodes, and internal flow configuration

Gas Phase Control Volume Equations. The exit gas temperature of each gas control volume of the reformer model is calculated using the conservation of energy equation

$$NC_v\frac{dT}{dt} = \dot{N}_{\text{in}}h_{\text{in}} - \dot{N}_{\text{out}}h_{\text{out}} + \sum \dot{Q}_{\text{in}} - \sum \dot{W}_{\text{out}} \tag{4}$$

where the constant volume specific heat capacity (C_v) is evaluated by subtracting the universal gas constant from the constant pressure specific heat capacity (C_p) as follows:

$$C_v(T) = \sum_i X_i \cdot C_p(T)_i - R \tag{5}$$

The constant pressure specific heat capacity is determined for the gas mixture as a function of temperature using Shomate coefficients. The number of moles in the gas control volume can be evaluated based on the ideal gas assumption:

$$N = \frac{PV}{RT} \tag{6}$$

The enthalpy of the gas is evaluated by accounting for sensible heat and the enthalpy of formation (h_f) directly

$$h = \sum_i X_i \cdot \left(\int_{T=298\ \text{K}}^{T} C_P(T)dT + h_f \right)_i \tag{7}$$

The corresponding exit species mole fractions are calculated using the following species conservation equation:

$$N\frac{dX_i}{dt} = \dot{N}_{\text{in}}X_{i,\text{in}} - \dot{N}_{\text{out}}X_{i,\text{out}} + R_i \tag{8}$$

The reaction rate (R_i) for the species in each gas control volume is specifically calculated on the basis of applicable chemical and/or electrochemical kinetics considering all species that are present and based on local variables (e.g., temperature, pressure). The fluid exit molar flow rate is determined based on the reaction rate as follows:

$$\dot{N}_{\text{out}} = \dot{N}_{\text{in}} + \sum_i R_i \tag{9}$$

Based on assumption 6, the pressure at the exit of each control volume is determined as follows:

$$P_{\text{out}} = P_{\text{in}} - \Delta P \tag{10}$$

The differences among the equations that are solved for in the specific SOFC, reformer, and combustor models are associated with the control volume definitions, material properties, heat transfer parameters and network, heat and work production within the control volume, and chemical and/or electrochemical kinetics considered.

Solution Strategy. The model makes use of the method of lines. Each of the components in the system model is discretized in space by using control volumes. In this fashion energy and species conservation equations are simplified into ordinary differential equations (Eqs. (1), (4), and (8)). These differential equations are solved by use of assumption 2, where the control volume temperature, pressure, and species mole fractions are assumed to be that of the exit conditions. From this assumption the energy conservation equations can be manipulated to obtain a state-space representation of temperature, and the species conservation equation can be manipulated to obtain a state-space representation of species mole fractions.

From the state-space representation of temperature and species mole fractions, the reaction rate, molar capacity, heat transfer, and thermodynamic properties can be evaluated avoiding algebraic loops. The molar flow rate, gas composition, gas pressure, and gas temperature are then passed from node to node for gas control volumes. The model predicts the dynamic performance of the integrated system, and resolves temperatures, species mole fractions, and flows as well as the extent of heat transfer and work generated locally throughout the system.

Detailed Component Model Descriptions

Reformer and Combustor. A geometrical schematic of the external steam reformer is presented in Fig. 2. The external steam reformer model, representing the experimental geometry, is comprised of three gas flow channels and a catalyst bed discretized into five nodes for a total of 20 control volumes. The inner flow channel is for steam (fuel cell depleted fuel), the middle annulus, which contains a nickel-alumina catalyst bed, is for reformate gas production, and the external annulus is for hot fuel cell exhaust. The physical parameters and specifications used in the external reformer model are presented in Table 1. The reformer does not generate work so the reformer model simultaneously solves a set of dynamic expressions that govern heat transfer and reformation chemical kinetics without work considered in the energy balance. Figure 3 shows the network of heat transfer within the reformer model.

The convection coefficients between gases and plates are determined by

$$h = \frac{\text{Nu}_D \cdot k_f}{D_H} \tag{11}$$

with the Nusselt numbers presented in Table 1 estimated from [18]. Heat transfer from the catalyst bed to the reformate gas is modeled as the heat transfer of gas as it passes through a bed of packed beads, where the resulting convection coefficient is evaluated from [18] as

Table 1 External steam reformer parameters used in the model

	Value	Units	Description
Reformer cans			
D_{Ecan}	0.185	m	Diameter of exhaust can
D_{Ccan}	0.176	m	Diameter of catalyst can
D_{Dcan}	0.137	m	Diameter of depleted fuel can
L	0.472	m	Length of reformer
Nu_{Dcan}	5.2648		Nusselt number for depleted fuel
Nu_{exch}	4.948		Nusselt number for exhaust gas
Catalyst ring			
D_{pe}	0.0173	m	External diameter of catalyst rings
D_{pi}	0.0084	m	Internal diameter of catalyst rings
H	0.010	m	Height of catalyst rings
ρ_s	2355.2	kg/m^3	Density of catalyst rings
d_p	0.0075	m	Catalyst ring equivalent sphere diameter
SA_{cat}	800	m^{-1}	Surface area to volume of the catalyst ring
Catalyst bed			
ε	0.528		Catalyst bed void fraction
C_{cat}	0.765	kJ/kg K	Specific heat capacity of bed
ρ_{bed}	1177.5	kg/m^3	Density of catalyst bed
k_s	0.036	kW/m K	Catalyst bed conduction coefficient
SA_{ref}	0.23504	m^2	Catalyst bed effective surface area

$$h = \frac{2.06 \cdot \mathrm{Re}_L \cdot \mathrm{Re}_D^{-0.575} \cdot k_f}{\varepsilon \cdot L \cdot \mathrm{Pr}^{1/3}} \tag{12}$$

The Reynolds number Re_D is defined in terms of the catalyst ring equivalent diameter and the equivalent empty channel (without packing) velocity

$$\mathrm{Re}_D = \frac{V \cdot d_p}{\upsilon} \tag{13}$$

The velocity through a control volume is determined in the model from the exit molar flow rate and the control volume molar concentration as follows:

$$V = \frac{\dot{N}_{\mathrm{out}}}{C \cdot CA} \tag{14}$$

Heat transferred axially through the reformer bed is evaluated as presented in [19] by summing the stagnant (k_{eo}), convection (k_{cv}), and radiation (k_r) conduction coefficients to determine the total effective bed conductivity. The conduction coefficients for this strategy are defined as follows:

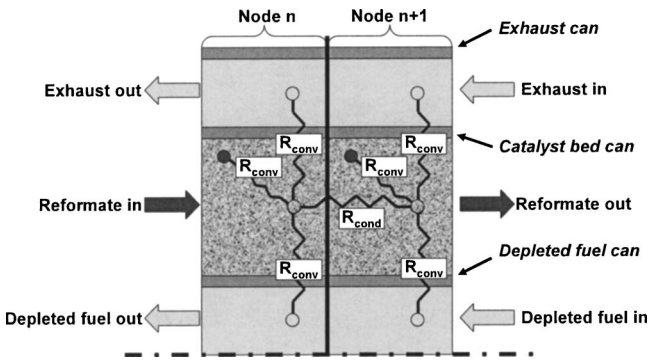

Fig. 3 Schematic of modeled heat transfer network within the external steam reformer

Stagnant:

$$k_{eo} = k_f \left(\left(1.814 \left(\frac{k_s}{(k_s - k_f)} \right)^2 \right) \cdot \left(\log\left(\frac{k_s}{k_f} \right) - \frac{(k_s - k_f)}{k_s} \right) + 0.0931 \right) \tag{15}$$

Convection:

$$k_{cv} = k_f (0.75 \cdot \mathrm{Pr} \cdot \mathrm{Re}_D) \tag{16}$$

Radiation:

$$k_{ro} = \frac{0.229 \cdot E \cdot \alpha \cdot d_p \cdot T^3}{1e^6} \tag{17}$$

$$k_r = \frac{(1-\alpha)}{\frac{1}{k_s} + \frac{1}{k_{ro}}} + \alpha + k_{ro} \tag{18}$$

Chemical kinetics for steam reformation in the reformer are based on the widely accepted chemical kinetic model presented in [20,21] which presents reaction rates for three chemical reactions

$$\mathrm{CH_4} + \mathrm{H_2O} \leftrightarrow 3\mathrm{H_2} + \mathrm{CO} \tag{19}$$

$$\mathrm{CO} + \mathrm{H_2O} \leftrightarrow \mathrm{CO_2} + \mathrm{H_2} \tag{20}$$

$$\mathrm{CH_4} + 2\mathrm{H_2O} \leftrightarrow \mathrm{CO_2} + 4\mathrm{H_2} \tag{21}$$

The combustor in the system is needed to convert fuel not utilized in the SOFC into heat. In addition, the SOFC air supply tube is routed through the combustor, in order to provide some cathode air preheating. The combustor model is comprised of one node with three control volumes: the reacting mixed fuel cell off-gas stream, a separator plate solid, and a cathode gas stream. Convective heat transfer between each of the control volumes is accounted for using Eq. (3). The corresponding reaction rates for each species (R_i) in the reacting stream are assumed fast enough to accomplish 100% oxidation of the fuel.

SOFC and Current Dissipater. A geometrical schematic of the resolved tubular cell is presented in Fig. 4. The simplified geometry of a single SOFC cell is solved numerically, with the results summed or multiplied to appropriately account for all 576 cells of the total 25 kW stack. The SOFC cell model consists of three gas flows: the inner for entering air, which then turns (180 deg) to become the cathode air in the middle channel, and the outer flow for the anode fuel stream as well as two solids: the air supply tube, and the fuel cell electrolyte assembly. The tubular fuel cell is discretized into ten nodes each containing three gas control volumes and two solid control volumes for a total of 50 control volumes. Sensitivity analyses of the number of nodes required to fully capture dynamic performance characteristics of the fuel cell have been performed previously suggesting that ten nodes is sufficient [22]. Physical parameters used in the SOFC tubular model are presented in Table 2.Within the SOFC model internal reformation, electrochemistry, work generation, and heat transfer are all solved simultaneously. Figure 5 shows the equivalent circuit network that describes heat transfer within the tubular SOFC model. Conduction and convection heat transfer are resolved using the set of parameters and constants presented in Table 2. Radiation heat transfer is modeled between the cell and air supply tube by modeling the tubes as long concentric cylinders as follows:

$$\dot{Q}_{\mathrm{rad}} = \frac{\sigma \cdot A (T_2^4 - T_1^4)}{\frac{1}{E_2} + \frac{1 - E_1}{E_1} \left(\frac{r_2}{r_1} \right)^2} \tag{22}$$

The fuel cell voltage in the model is found in a typical way by subtracting locally calculated activation, ohmic, and concentration polarizations from the locally calculated Nernst potential. The

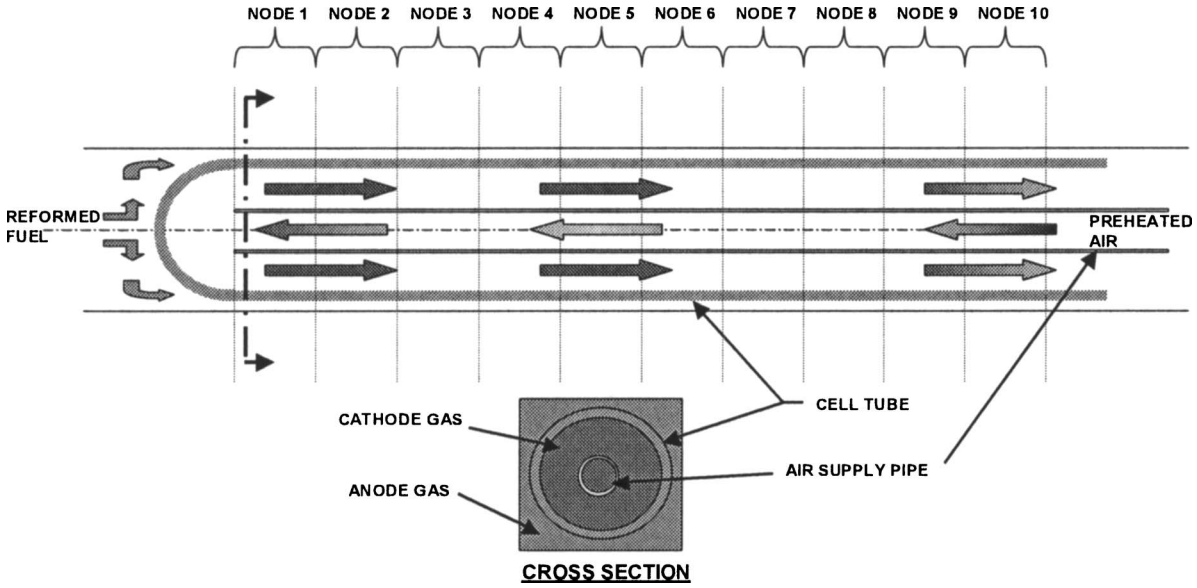

Fig. 4 Schematic of a Siemens Westinghouse tubular SOFC, showing model nodes, and internal flow configuration

Nernst equation is solved for both the anode and cathode partial pressures, and the reversible potential dependence is accounted for by solving the dependence of Gibbs free energy on temperature.

$$V_{\text{Nernst}} = -\frac{\Delta G(T)}{n \cdot F} + \frac{R \cdot T}{n \cdot F} \ln\left[\frac{P_{H_2} \cdot P_{O_2}^{1/2}}{P_{H_2O}}\right] \tag{23}$$

The activation polarization is from [17]

$$E_{\text{Act}} = \frac{R \cdot T}{n \cdot F} \ln\left(\frac{i/A}{i_o(T)}\right) \tag{24}$$

Where the exchange current density i_o is that of the cathode based on temperature from [17] as well. Ohmic polarization was evaluated by using the equivalent resistance presented in Table 2. The equivalent resistance was determined to represent an average cell performance at the nominal operating temperature, capturing the ionic resistance in the anode, electrolyte, and cathode as well as the electronic resistance in the electrodes and stack interconnects. While the resistance is temperature dependent in general, the current research focuses on the relatively constant temperature operation of the Siemens Westinghouse 25 kilowatt system. As a result, resistance was assumed constant in this study. Concentration polarization is approximated by

$$E_{\text{conc}} = -\frac{R \cdot T}{n \cdot F} \ln\left(1 - \frac{i/A}{i_l}\right) \tag{25}$$

The voltage is determined at each node, but to satisfy the equipotential assumption, at each time step a cell voltage is fixed and each nodal current is then iterated until each node voltage is equal to the cell voltage. The nodal currents are then added and multiplied by the external resistance to determine the next time step cell voltage. The external resistance is determined in a dissipater model, where the external resistance can be changed using a feedback loop that controls the fuel cell current, power, or voltage depending on the case simulated. Electrochemical reactions, steam reformation reactions, and water gas shift reactions are all considered in the fuel cell. Internal steam reformation and water gas shift chemical kinetic rates are solved in the fuel cell based on [20,21] as was done in the reformer model. However, because the fuel cell generally operates at a relatively high temperature for reformation (1000°C), a water gas shift equilibrium condition is applied to the exit condition of each anode control volume (following the chemical kinetics). In this fashion each node in the fuel cell resolves steam reformation kinetics, and water gas shift equilibrium. Because of assumption 15 only hydrogen is electrochemically reacted in the anode compartment, which provides the following electrochemical reaction in the anode:

$$H_2 + O^{2-} \rightarrow H_2O + 2e^- \tag{26}$$

The following electrochemical reaction in the cathode:

$$\frac{1}{2}O_2 + 2e^- \rightarrow O^{2-} \tag{27}$$

which reaction rates are determined as

$$\text{rate} = \frac{i}{n \cdot F} \tag{28}$$

Energy of reaction for both the internal reformation and electrochemistry are directly accounted for in the gases by solving for enthalpy in the energy conservation Eq. (7). Irreversibilities in the

Table 2 SOFC tubular cell parameters used in the model

Stack	Value	Units	Description
Series	192		Number of cells in series
Parallel	3		Number of cells in parallel
Cell			
D_A	0.0159	m	Cell outside diameter
D_C	0.0118	m	Cell inner diameter
OD_{asp}	0.0055	m	Air supply pipe outside diameter
ID_{asp}	0.0045	m	Air supply pipe inner diameter
L	0.5	m	Cell length
ρ_{asp}	3970	kg/m^3	Air supply pipe density
ρ_e	1500	kg/m^3	Electrolyte solid density
C_{asp}	0.765	kJ/kg K	Air supply pipe specific heat capacity
C_e	0.8	kJ/kg K	Electrolyte specific heat capacity
h_a, h_c, h_{asp}	0.05	kW/m^2 K	Anode, cathode, and asp convection coefficient
k	0.006	kW/m K	Cell conduction coefficient
E_{asp}	0.55		Air supply pipe emissivity
Ee	0.8		Electrolyte emissivity
i_l	8000	A/m^2	Fuel cell limiting current density
R_{eq}	0.000027	ohm m^2	Fuel cell equivalent internal resistance

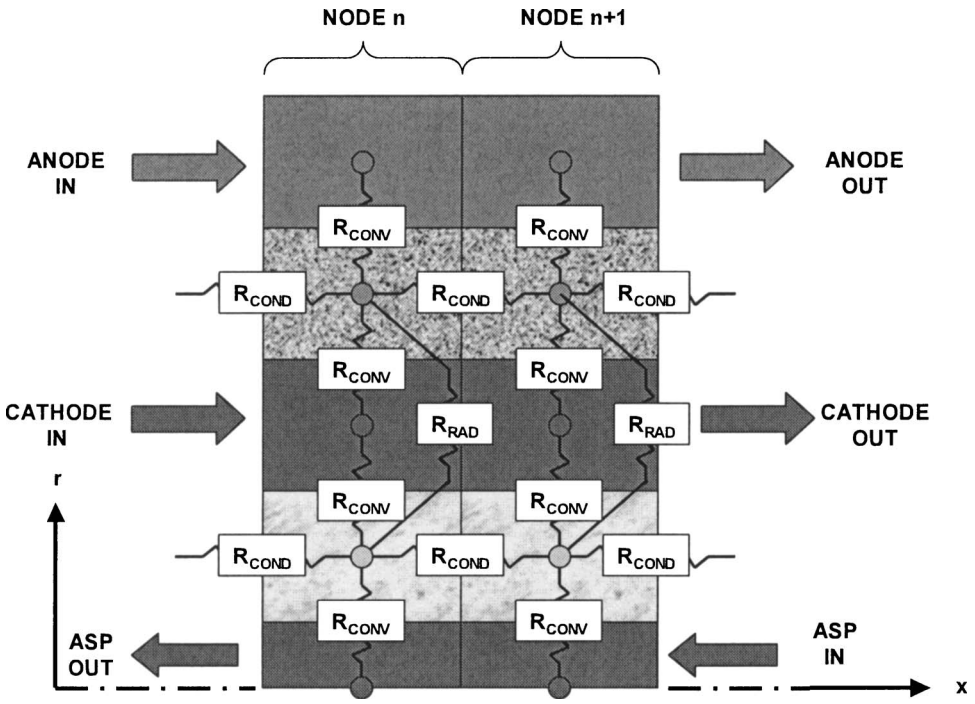

Fig. 5 Schematic of modeled heat transfer network within the tubular SOFC

fuel cell are modeled as heat generated in the electrolyte solid. Work generation, and its corresponding generated heat are appropriately captured in the model by removing all of the product water enthalpy of formation based on the temperature of the electrolyte from the anode stream.

$$\dot{W}_{\text{out}} = h_{f(\text{H}_2\text{O})}(T_e)\frac{i}{n \cdot F} \tag{29}$$

The difference in energy between the product water enthalpy of formation and power generated by the fuel cell is considered heat generated in the electrolyte solid.

$$\dot{W}_{\text{out}} = -\left(h_{f(\text{H}_2\text{O})}(T_e)\frac{i}{n \cdot F} - iV\right) \tag{30}$$

This difference represents heat generated due to entropy generation of the electrochemical reaction, as well as losses due to the activation, ohmic, and concentration polarizations.

The set of equations presented herein is the complete set of equations used in the model. All equations that represent the fuel cell and the system as a whole are simultaneously solved using built-in SIMULINK solvers to simulate the system dynamically.

Results

Model Comparison to Data. The integrated system model developed in this work simulates the experimental 25 kW SOFC system of Siemens Westinghouse Power Corporation stationed at the National Fuel Cell Research Center. The simulation results can therefore be compared to data acquired from this real system, with some limitations. The limitations are due to the fact that the system is designed to operate at steady state at one of four operating points, and the sampling rate of system performance data is only at one minute resolution. As a result, only steady-state comparisons can be made. By setting the current, fuel flow rate, and inlet air flow rates to those of the physical system, the model was able to predict the experimental system power to within 3%, and the center cell temperature to within 5% throughout the range of operation as presented in Fig. 6. Note that the simulation temperature is compared to the system set-point temperature in Fig. 6. This temperature was selected for comparison since the measured physical system temperature varies throughout the stack with an average measured temperature corresponding well to this set point.

Simulated Open Loop Response. The dynamics of the system power response to an instantaneous lowering of the system external resistance by 5% was investigated in order to understand the system power dynamic response characteristics following a power change. In the simulation, the dynamic model was first allowed to reach steady state at the nominal power setting before the instantaneous perturbation in load resistance was applied. No other changes in inputs, such as the fuel flow or air flow were made to the system so that its open loop response to this perturbation alone could be studied.

The simulation captured two distinct responses, a fast response due to the change in concentration as presented in Fig. 7 and a much slower response due to temperature change as presented in Fig. 8. Note that the model does not capture dynamics associated with electrochemistry and power electronics because of the quasisteady electrochemistry assumption and the power electronics

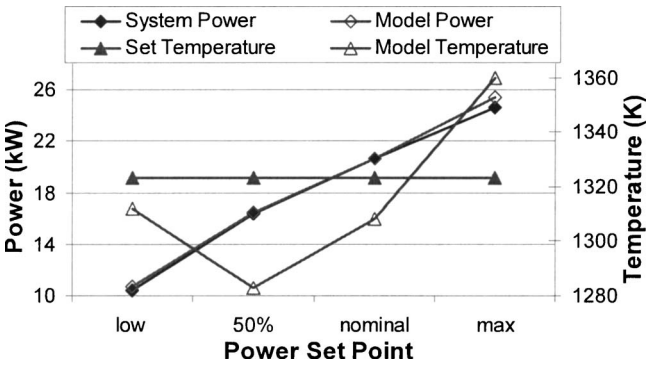

Fig. 6 Comparison of power and temperature data to system simulation output results

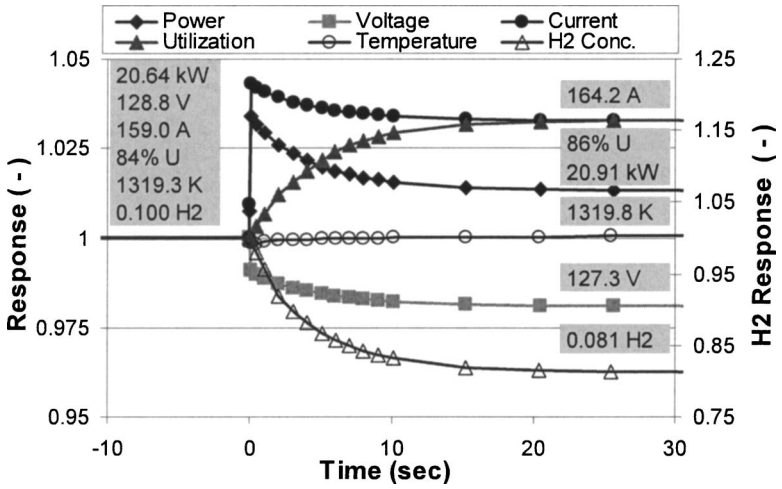

Fig. 7 Typical open loop response of power, voltage, current, fuel utilization, center cell temperature, and fuel cell exit hydrogen concentration following a load resistance drop of 5%. Data normalized to initial steady state conditions.

solution technique. The model did capture the important response of the fuel cell system due to hydrogen and temperature variations as presented in literature [10].

The slight fuel cell temperature rise over time as shown in Fig. 8 is due to the increased current following the load resistance drop. An increase in current results in additional ohmic, activation, and concentration losses, which adds heat generation in the stack. Since the air and fuel flow rates were not increased, the stack temperature slowly increased. The temperature increase in the system is very slow due to the systems large thermal capacity. The extra heat in the stack slowly heats up the reformer and the combustor as well as the stack. The primary finding is that fuel cell voltage, current, and power respond quickly to the load resistance change as plotted in Figs. 7 and 8, while the temperature changes over a much larger time scale with much smaller impact on fuel cell performance.

Fuel cell temperature transients are very important to understand and control since SOFC stack materials are sensitive to temperature change and gradients. Due to large thermal response time, on the order of minutes, fuel cell temperature can be controlled by manipulating the air flow rate to remove excess heat. The challenge lies in how one can address the delay between air flow set point change and resultant temperature change. For brevity, temperature controllers are not explored in this paper. Instead we focus on the faster anode hydrogen concentration transients, on the order of seconds. As shown in Fig. 7, the temperature of the fuel cell does not change during the time of the hydrogen transient. As a result, the effect of temperature can be ignored while analyzing hydrogen transients due to load change.

The SOFC system power, voltage, current, and internal hydrogen concentration dynamic response to an instantaneous load resistance change can be explained physically. The fuel cell voltage is dependent on the fuel cell operating hydrogen concentration, current, and temperature, and does not change directly due to a change in load resistance. However, the current is directly dependent on the resistance, and instantaneously rises due to the external resistance change. The increase in current causes the voltage to instantaneously decrease, due to additional polarization. The increase in fuel cell current also results in consumption of hydrogen, as shown in Eq. (26). Due to reactant mass storage within the

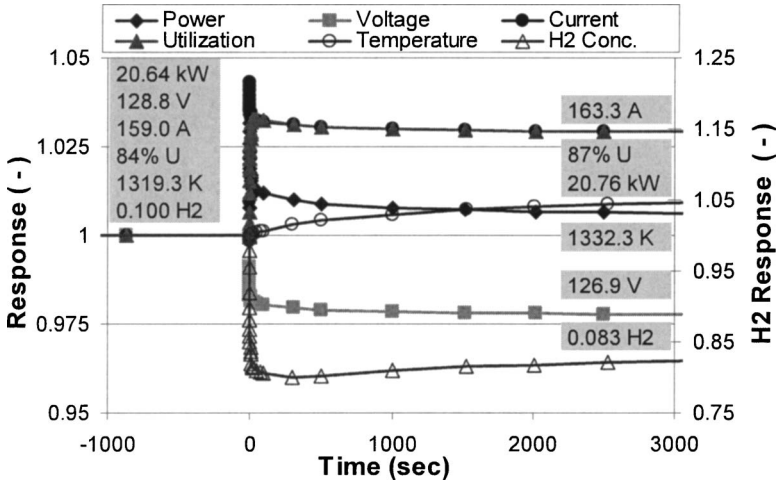

Fig. 8 Typical open loop response of power, voltage, current, fuel utilization, center cell temperature, and fuel cell exit hydrogen concentration following a load resistance drop of 5%. Data normalized to initial steady state conditions.

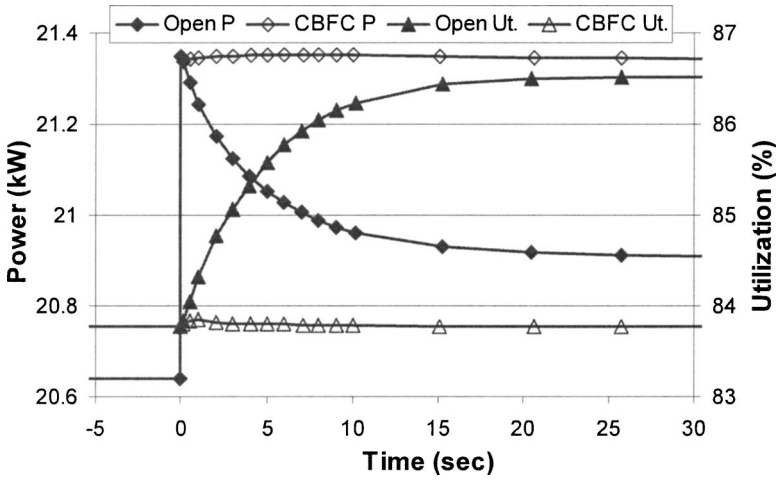

Fig. 9 Comparison of the power and fuel utilization results from the open loop (open) and current-based flow control (CBFC) system dynamic response

cell and the concurrent solution of mass transport and conservation equations (that include the hydrogen electrochemical sink) the hydrogen concentration will slowly decrease with time throughout the cell. Due to the transient reduction of hydrogen concentration in the fuel cell, the voltage decreases with time.

The transient in power can be described by

$$P = i \cdot V = \frac{V^2}{R_e} \tag{31}$$

The power out of the fuel cell instantaneously increases due to the instantaneous decrease in load resistance, and then slowly lowers with time as the voltage decreases. The power transient response is thus similar to the transient in voltage, which tracks the reduction of hydrogen concentration within the fuel cell. The decrease in hydrogen concentration thus significantly contributes to the transient and reduction in system power.

Current-Based Fuel Control (CBFC) Simulations. To minimize dynamics during system load changes, it is desired to maintain the hydrogen concentration within the fuel cell. The hydrogen concentration in the fuel cell is difficult to measure or determine, since it depends on the amount of hydrogen being reacted electrochemically, the extent of reformation reactions, temperature, and many other factors. A fully detailed model, as presented in this paper, is required to calculate hydrogen concentrations. Since these types of predictive modeling tools are not desired for use in control strategies, we choose instead to control the overall amount of available hydrogen in the fuel cell.

In order to do this, we investigated utilization based on the current as follows:

$$U = \frac{i \cdot \text{series}}{\dot{N}_{\text{in}}(X_{H_2} + X_{CO} + 4X_{CH_4})_{\text{in}} n \cdot F \cdot 1000} \tag{32}$$

Where series is the number of cells in series, and

$$X_{H_2} + X_{CO} + 4X_{CH_4} \tag{33}$$

represents the concentration of available hydrogen in the fuel stream since from Eqs. (19)–(21) one mole of methane produces four moles of hydrogen and one mole of carbon monoxide can produce one mole of hydrogen. This hydrogen availability concept is possible because other reactions that could take place in the reformer are assumed negligible (a good assumption).

Equation (32) suggests that utilization will remain constant if the fuel flow rate into the system is controlled proportionally to current as follows:

$$\dot{N}_{\text{fuel}} = \frac{i \cdot \text{series}}{U_{\text{sel}}(X_{H_2} + X_{CO} + 4X_{CH})_{\text{in}} n \cdot F \cdot 1000} \tag{34}$$

The number of cells in series and system inlet fuel concentration should be constant. Thus, as long as the inlet fuel composition is known, the electrochemical reactions generate their ideal number of electrons and no fuel crosses the electrolyte, controlling the fuel flow rate by Eq. (34) allows for control of fuel utilization (and hydrogen availability in the fuel cell). Note that in this control strategy the operating utilization (U_{set}) is an input to the control strategy. This strategy for controlling the fuel flow rate is called current-based fuel control (CBFC) in this paper.

To give insight to this control strategy, we investigated the transients involved with utilization defined in a more typical way as ratios of species mole fraction

$$U = 1 - \frac{\dot{N}_{\text{out}}(X_{H_2} + X_{CO} + 4X_{CH_4})_{\text{out}}}{\dot{N}_{\text{in}}(X_{H_2} + X_{CO} + 4X_{CH_4})_{\text{in}}} \tag{35}$$

This utilization is entirely based on fuel concentration, and will change with transients in hydrogen concentration within the fuel cell while the current-based utilization (Eq. (32)) will not. We developed our control strategy based on utilization defined by current (Eq. (32)), but we plotted and discussed the response of utilization based on ratios of species mole fraction (Eq. (35)).

To demonstrate the effectiveness of current-based fuel control, the simulation of instantaneously lowering the external load resistance by 5% was repeated with the fuel flow rate controlled by Eq. (34) to maintain constant fuel utilization. The response of utilization and power generation is plotted in Fig. 9 in comparison with the open loop response to the same transient. Current-based fuel control adjusted the amount of fuel supplied to the fuel cell, and minimized transient in the fuel cell power response.

Physically, current-based fuel control is replenishing the fuel cell with the same amount of fuel that is being consumed. Since we are assuming incompressible flow, and constant pressure drop throughout the system (assumption 6), changes in fuel flow rate will affect the system instantaneously. As a result, CBFC replenishes the fuel cell with new fuel as fast as it is consuming fuel, resulting in constant fuel utilization. In addition, the current reformer is sufficiently large and has negligible pressure drop allowing it to process the fuel effectively throughout the transient (resulting in consistent outlet reformate composition). Thus,

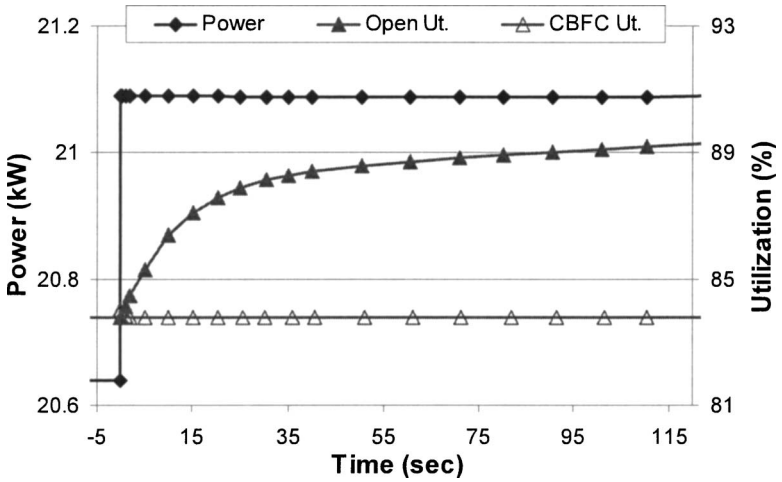

Fig. 10 Power and fuel utilization transients from the open loop (open) and current-based flow control (CBFC) following a simulated instantaneous 2.2% change in power

controlling the fuel flow by CBFC has removed the cause of the gradual decrease in power of the open loop case (i.e., lower concentrations, leading to lower Nernst voltage, leading to lower power).

These results (Fig. 9) establish an important fundamental understanding that a well-designed reformer and good controls can enable rapid SOFC system load-following capability. The performance shown in Fig. 9 may not be generally true for other system designs, depending upon reformer design and performance. In practice the requirements of low pressure drop, negligible flow delays, consistent reformate composition, as well as rapid fuel flow actuation and current sensing required for the performance as illustrated above, could be challenging during dynamic operation of an integrated fuel cell system. These difficulties and/or other complications can result in delays in fuel actuation. The implications of such delays are addressed in a subsequent section of this paper.

Fuel cell systems in the built environment will generally be controlled by power. Inverters will draw as much current as needed to meet the power demand. It is therefore desired to compare the performance of the fuel cell system controlled by power without fuel flow control, to the performance of the same system controlled by power with current-based fuel flow control. This was accomplished by simulating an instantaneous 2.2% power increase for the system for two cases. One with no fuel flow change, and another with fuel flow rate change by CBFC. The simulation shows that in both cases, the power will change in a lock-step fashion as shown in Fig. 10.

Even though the fuel cell with no change in fuel flow appears able to meet the step change load demand, the fuel utilization increased dramatically in the fuel cell as shown in Fig. 10. This is problematic because if the step change in power was made an additional 0.1% larger, the fuel cell hydrogen would have been completely depleted. This is because of nonlinear decreases in voltage due to effects of concentration in the Nernst equation and electrochemical loss terms within the fuel cell. As hydrogen concentration goes down in the fuel cell, the fuel cell voltage lowers, causing the power electronics to draw more current, which in turn further lowers the hydrogen concentration until no hydrogen remains in the fuel cell. By changing the fuel flow rate in proportion to the current as described by Eq. (34), simulations show that available hydrogen concentration within the fuel cell remains almost constant.

CBFC resolves the problem of maintaining hydrogen concentration within the fuel cell during transients. The CBFC control strategy does have limitations however. For example, there might be a significant time delay between the time an increase in current is sensed to the time new fuel is fed to the system by a mass flow controller or valve. The effects of such a delay were investigated by simulating a 0 sec, 2 sec and 5 sec flow response delay as described above for a set of simulated dynamic responses to a 10% instantaneous power increase perturbation. In each of these simulations, the power electronics followed the step change exactly, but due to the delay in fuel flow actuation the fuel utilization increased before the new fuel was available as shown in Fig. 11. This simulation shows that system gas transport delays are not as important to system dynamic response as are the delays in the controller, and valves. A 5 s delay may be longer than a typical valve/controller response. Nonetheless, the simulation results presented in Fig. 11 show that problematic high utilization can rather easily result in a fuel cell if fuel flow is not carefully controlled during load transients. This depletion of hydrogen can come with severe consequences to the fuel cell including the potential permanent degradation of performance due to anode oxidation. The implications of the simulated delay emphasize that further work is needed.

Summary and Conclusions

In order to understand and improve fuel cell transient capability a system model of an integrated SOFC system, a Siemens Westinghouse 25 kW tubular SOFC, was developed. The dynamic system model was created by integrating system component models based on conservation equations, and semiempirical relations. The model was shown to predict the actual system within 3% accuracy in power, and 5% accuracy in temperature. The model was further used to analyze the characteristic transients of the system. High utilization (low hydrogen concentration) was found to be problematic when fuel flows are not changed during power transients. To solve this problem current-based fuel control was proposed and shown to minimize transients in utilization and stabilize the response of the fuel cell. In this control strategy fuel actuator response time was shown to be a major limitation to fuel cell transient capability.

Simulations of the system have shown that with a detailed understanding of fuel cell system response, control strategies can be developed to greatly increase fuel cell load following capability. With controls development fuel cell systems should be capable of rapid load following capabilities, which will probably be limited by actuator response times.

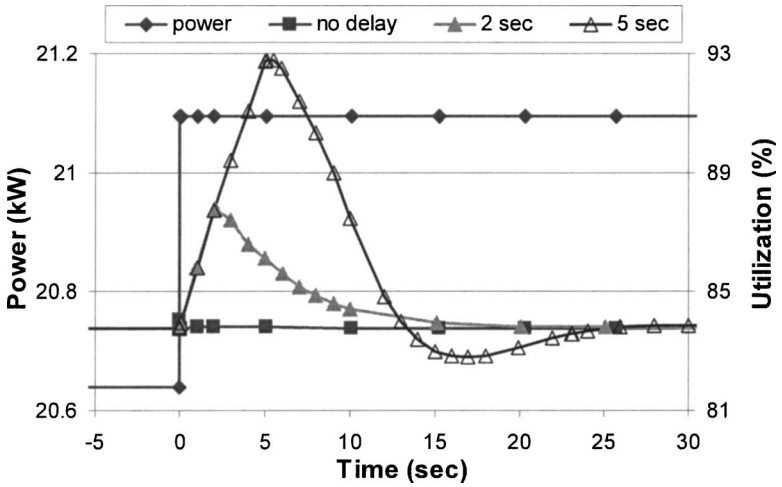

Fig. 11 Power and fuel utilization transients, due to flow delay in current-based flow control strategy following a large instantaneous power change

Acknowledgment

We acknowledge the financial support of the California Energy Commission, which partially sponsored this effort, and contributions of Arthur J. Soinski, Ph.D., Contract Manager. This paper was prepared in part as a result of work sponsored by the California Energy Commission (Commission). It does not necessarily represent the views of the Commission, its employees, or the State of California. The Commission, The State of California, its employees, Contractors, and Subcontractors make no warranty, expressed or implied, and assume no legal liability for the information in this paper; nor does any party represent that the use of this information will not infringe upon privately owned rights. This paper has not been approved or disapproved by the Commission nor has the Commission passed upon the accuracy or adequacy of the information in this paper.

Nomenclature

A = surface area (m^2)
C = solid specific heat capacity ($kJ\,kg^{-1}\,K^{-1}$), molar concentration of control volume ($kmol\,m^{-3}$)
CA = cross-sectional area (m^2)
D_H = hydraulic diameter (m)
d_p = reformer catalyst equivalent sphere diameter (m)
E = emissivity (-), polarization (V)
F = Faraday's constant ($96,487\ C\,mol^{-1}$)
ΔG = change in Gibbs free energy of formation ($kJ\,kmol^{-1}$)
h = enthalpy ($kJ\,kmol^{-1}$), convective heat transfer coefficient ($kW\,m^{-2}\,K^{-1}$)
i = electrical current (A)
i_o = exchange current density ($A\,m^{-2}$)
i_l = limiting current density ($A\,m^{-2}$)
k_f = fluid conduction heat transfer coefficient ($kW\,m^{-1}\,K^{-1}$)
k_s = solid conduction heat transfer coefficient ($kW\,m^{-1}\,K^{-1}$)
L = length (m)
N = molar capacity, or total number of moles (kmol)
$\dot{N}$ = molar flow rate ($kmol\,sec^{-1}$)
n = number of participating electrons in the reaction (-)
Nu_D = Nusselt number (-)
P = power (kW), pressure (Kpa)
P_i = partial pressure of gas (atm)
Pr = Prandtl number (-)
$\dot{Q}$ = heat transfer (kW)
R = universal gas constant ($8.3145\ kJ\,kmol^{-1}\,K^{-1}$), control volume reaction rate ($kmol\,sec^{-1}$)
r = radius (m)
Re_L = Reynolds number (-)
Re_D = Reynolds number based on particle diameter (-)
R_e = electrical resistance (ohm)
T = control volume temperature (K)
t = time (sec)
U = fuel utilization (-)
V = volume (m^3), voltage (V), velocity ($m\,sec^{-1}$)
$\dot{W}_{out}$ = work out of control volume (kW)
X = species mole fraction (-)

Greek Letters

α = absorptivity (-)
ϵ = catalyst bed void fraction (-)
σ = Stefan-Boltzmann constant ($5.67\times10^{-8}\ W\,m^{-2}\,K^{-4}$)
ρ = density of solid ($kg\,m^{-2}$)
υ = kinematic viscosity ($m^2\,sec^{-1}$)

Superscripts

a = anode gas control volume
asp = air supply pipe solid control volume
c = cathode gas control volume
e = electrolyte solid control volume

References

[1] Jurado, F., Valverde, M., and Cano, A., 2004, "Effect of a SOFC Plant on Distribution System Stability," J. Power Sources, **129**, pp. 170–179.
[2] Nickens, A., Cervi, M., Abens, S., and Hoffman, D., 2004, "US Navy Ship Service Fuel Cell Program," *Fuel Cell Seminar*, San Antonio, Texas.
[3] Stevenson, J. W., Khaleel, D. L., King, G. L., and McVay, P. S., 2004, "Solid Oxide Fuel Cell Development Activities at Pacific Northwest National Laboratory," *Fuel Cell Seminar*, San Antonio, Texas.
[4] Eelman, S., and Poza, I. P., 2004, "Fuel Cell APU's in Commercial Aircraft-An Assessment of SOFC and PEMFC Concepts," *24th International Congress of the Aeronautical Sciences*, Yokohama, Japan.
[5] Randall, S. G., Liese, E., Riveria, J. G., Jabbari, F., and Brouwer, B., 2000, "Development of Dynamic Modeling Tools For Solid Oxide and Molten Carbonate Hybrid Fuel Cell Gas Turbine Systems," *International Gas Turbine and Aeroengine Congress and Exhibition*, Munich Germany, May 8–10, ASME Paper No. 2000-GT-0554.

[6] Peters, D., Freeh, L., Kopasakis, G., and Steffens, C., 2004, "Fuel Cell System Modeling and Analysis at the NASA Glenn Research Center," *Fuel Cell Seminar*, San Antonio, Texas.
[7] Haynes, C., 2004, "An Investigation to Resolve the Interaction Between SOFC Module, PES, and Balance-of-Plant During Transient Conditions," *Fuel Cell Seminar*, San Antonio, Texas.
[8] Lim, D. S., Brouwer, J., Neylon, M. K., Fleckner, K. M., Finalyson, B. A., and Loffler, D. G., 2004, "Novel Integrated Use of Femlab and Simulink to Understand the Dynamics of an SOFC/ Reformer System for Aeronautical Applications," *Fuel Cell Seminar*, San Antonio, Texas.
[9] Roberts, R. A., Brouwer, J., and Samuelsen, G. S., 2004, "Dynamic Simulation of a Solid Oxide Fuel Cell/Gas Turbine Hybrid and Comparison to Data," *Fuel Cell Seminar*, San Antonio, Texas.
[10] Dicks, A. L., and Martin, P. A., 1998, "A Fuel Cell Balance of Plant Test Facility," J. Power Sources, **71**, pp. 321–327.
[11] Yi, Y., Brouwer, J., Rao, A. D., and Samuelsen, G. S., 2004, "Fuel Flexibility Study of an Integrated 25 kW SOFC Reformer System," *Fuel Cell Seminar*, San Antonio, Texas.
[12] Casanova, A., 1998, "A consortium Approach to Commercialized Westinghouse Solid Oxide Fuel Cell Technology," J. Power Sources, **71**, pp. 65–70.
[13] Burt, A. C., Celik, I. B., Gemmen, R. S., and Smirnov, A. V., 2004, "A Numerical Study of Cell to Cell Variation in a SOFC Stack," J. Power Sources, **126**, pp. 76–87.
[14] Campanari, S., and Iora, P., 2004, "Definition and Sensitivity Analysis of a Finite Volume SOFC Model for a Tubular Cell Geometry," J. Power Sources, **132**, pp. 113–126.
[15] Andrew, M. R., 1966, "Kinetic Effects-Part 2," *An Introduction to Fuel Cells*, K. R. Williams, ed., Elsevier Publishing Company, New York, Chap. 4.
[16] Srinivasan, S., Omourtag, A. V., Parthasrathy, A., Manko, D. J., and Appleby, A. J., 1991, "High Energy Efficiency and High Power Density Proton Exchange Membrane Fuel Cells-Electrode Kinetics and Mass Transport," J. Polym. Sci., Polym. Symp., **36**, pp. 299–320.
[17] Bessette, N. F., 1994, "Modeling and Simulation for Solid Oxide Fuel Cell Power Systems," Ph.D. thesis, Georgia Institute of Technology, Atlanta.
[18] Incropera, F. P., and Dewitt, D. P., 2002, *Fundamental of Heat and Mass Transfer*, Wiley, New York.
[19] Gabor, J. D., and Botterill, J. S. M., 1985, "Heat Transfer in Fluidized and Packed Beds," *Handbook of Heat Transfer Applications*, 2nd ed. W. M. Rohsenoe, et al., eds., McGraw-Hill, New York.
[20] Xu, J., and Froment, G. F., 1989, "Methane Steam Reformation, Methanation and Water-Gas Shift: I. Intrinsic Kinetics," AIChE J., **35**(1), pp. 88–96.
[21] Xu, J., and Froment, G. F., 1989, "Methane Steam Reforming: Diffusional Limitations and Reactor Simulation," AIChE J., **35**(1), pp. 97–103.
[22] Gemmen, R., Liese, E., Rivera, J., Jabbari, F., and Brouwer, J., 2000, Development of Dynamic Modeling Tools for Solid Oxide and Molten Carbonate Fuel Cell Gas Turbine Systems, ASME Paper Number 2000-GT-554, May.